Probing Lipid Mobility of Raft-exhibiting Model Membranes by Fluorescence Correlation Spectroscopy*

Nicoletta Kahya‡§, Dag Scherfeld‡, Kirsten Bacia‡, Bert Poolman¶‖, and Petra Schwille‡

From the ‡Experimental Biophysics Group, Max Planck Institute for Biophysical Chemistry, Am Fassberg 11, 37077 Göttingen, Germany and the ¶Membrane Enzymology Group, University of Groningen, Nijenborgh 4, 9747 AG Groningen, The Netherlands

Confocal fluorescence microscopy and fluorescence correlation spectroscopy (FCS) have been employed to investigate the lipid spatial and dynamic organization in giant unilamellar vesicles (GUVs) prepared from ternary mixtures of dioleoyl-phosphatidylcholine/sphingomyelin/cholesterol. For a certain range of cholesterol concentration, formation of domains with raft-like properties was observed. Strikingly, the lipophilic probe 1,1′-dioctadecyl-3,3,3′,3′-tetramethylindocarbocyanine perchlorate (DiI-C₁₈) was excluded from sphingomyelin-enriched regions, where the raft marker ganglioside GM1 was localized. Cholesterol was shown to promote lipid segregation in dioleoyl-phosphatidylcholine-enriched, liquid-disordered, and sphingomyelin-enriched, liquid-ordered phases. Most importantly, the lipid mobility in sphingomyelin-enriched regions significantly increased by increasing the cholesterol concentration. These results pinpoint the key role, played by cholesterol in tuning lipid dynamics in membranes. At cholesterol concentrations >50 mol%, domains vanished and the lipid diffusion slowed down upon further addition of cholesterol. By taking the molecular diffusion coefficients as a fingerprint of membrane phase compositions, FCS is proven to evaluate domain lipid compositions. Moreover, FCS data from ternary and binary mixtures have been used to build a ternary phase diagram, which shows areas of phase coexistence, transition points, and, importantly, how lipid dynamics varies between and within phase regions.

More than 10 years ago, the hypothesis was formulated that cellular membranes are organized in discrete dynamic entities, called lipid rafts (1, 2). Studies on epithelial cell polarity revealed that lipids, in particular sphingolipids and cholesterol, were laterally organized in the exoplasmic leaflet of the apical plasma membrane according to a variable short and long range order. Furthermore, distinct proteins were shown to selectively partition into lipid rafts, indicating that rafts could serve as specific sites for molecular sorting and polarized transport. They also function as platforms for intra- and intercellular signaling (3, 4), *e.g.* in T-cells and basophils (5–10), and play an important role in sorting, occurring in the *trans*-Golgi network

of polarized epithelial cells (1, 11, 12) and neurons (13), as well as in pathways originating from the cell surface, *i.e.* involving caveolae (14, 15) and endocytic pathways (3, 12, 16). In addition, rafts may be important in cell surface proteolysis (17) and virus infection (18).

Commonly, lipid rafts are enriched in sphingolipids and cholesterol (1–4). The presence of long and saturated acyl chains in sphingolipids allows cholesterol to become tightly intercalated with such lipids, resulting in the organization of liquid-ordered (l_o) phases. By contrast, unsaturated phospholipids are loosely packed and form a disordered state (usually indicated as liquid crystalline l_c or liquid-disordered l_d) (19, 20). The difference in packing ability leads to phase separation (21, 22). Model membrane studies carried out on ternary mixtures of cholesterol with phospholipids and sphingolipids show that l_o phases, enriched in sphingolipids, separate from l_d phases, enriched in phospholipids (19, 23). Several observations indicate that these "artificial rafts" are a reasonable, though crude, model of raft-containing cell membranes (24).

More recently, along with a number of techniques employed to address questions on rafts (11, 21, 25–27), important contributions have also come from optical microscopy (28, 29). Direct visualization of raft-like domains in model bilayer membranes has provided a tangible proof for the coexistence of liquid-ordered and liquid-disordered phases (30–33). However, rafts are by no means static structures. If it is true that their main function consists of forming platforms to concentrate certain proteins, then a detailed characterization of lipid and protein dynamics in the different phases is essential to understand mobility-dependent protein organization (34). Single particle tracking (SPT) has been applied to follow raft-associated proteins *in vivo* (29) and lipid mobility in cell membranes and *in vitro* (31, 35). Additional contributions have come from fluorescence recovery after photobleaching (FRAP) (32) and fluorescence resonance energy transfer (FRET) (28). However, a detailed characterization of cholesterol-containing membranes from a dynamic point of view is still lacking.

Fluorescence correlation spectroscopy (FCS)[1] is based on the time-correlation of temporal fluorescence fluctuations detected in the focal volume, which are governed by dynamic parameters of the system at equilibrium (36, 37). The power of FCS relies on the single molecule sensitivity and the capability of exploring a wide range of dynamic events with high temporal resolution and good statistical accuracy (38). In the past, this technique has been proven to be a powerful tool to follow lipid

---

[1] The abbreviations used are: FCS, fluorescence correlation spectroscopy; GUVs, giant unilamellar vesicles; LUVs, large unilamellar vesicles; DOPC, L-α-dioleoyl-phosphatidylcholine; SM, N-stearoyl-D-erythrosphingosylphosphorylcholine; DiI-C₁₈, 1,1′-dioctadecyl-3,3,3′,3′-tetramethylindocarbocyanine perchlorate; MβCD, methyl-β-cyclodextrin; ITO, indium tin oxide.

dynamics in domain-forming giant unilamellar vesicles (GUVs) (39), which serve as excellent model membranes for single molecule optical microscopy (40).

In this study, we present a detailed characterization of lipid dynamics in raft-forming GUVs prepared from a ternary mixture of cholesterol, dioleoyl-phosphatidylcholine, and sphingomyelin. By combining confocal optical microscopy and FCS, insight is gained in the static and dynamic organization of lipids, partitioning in different phases. It is evident that cholesterol plays a key role in promoting raft formation and, most importantly, in tuning membrane lipid mobility. Finally, we show that FCS provides information on lipid raft composition, allowing for a mapping of the lipid phase diagram, entirely based on dynamic parameters.

MATERIALS AND METHODS

Chemicals—1,2-Dioleoyl-sn-glycero-3-phosphocholine (dioleoyl-phosphatidylcholine; DOPC), N-stearoyl-D-erythrosphingosylphosphorylcholine (stearoyl sphingomyelin, SM), cholesterol, porcine brain ganglioside GM1 (GM1) were purchased from Avanti Polar Lipids. 1,1′-Dioctadecyl-3,3,3′,3′-tetramethylindocarbocyanine perchlorate (DiIC$_{18}$) and the Alexa-Fluor 488 conjugate of cholera toxin B subunit (AF-CTB) were from Molecular Probes. The cholesterol-sequestering agent methyl-β-cyclodextrin (MβCD) was from Sigma. All other chemicals were of reagent grade.

Preparation of GUVs—GUVs were prepared by electroformation (40, 41). With this approach, truly unilamellar vesicles are produced with sizes varying from 10 up to 100 μm (42, 43). The flow chamber (closed-bath perfusion chamber, RC-21, Warner Instruments Co.) used for vesicle preparation was equipped with two microscope slides, each coated with optically transparent and electrically conductive indium tin oxide (ITO). Lipids in chloroform/methanol 9:1 (5 mM, prepared freshly and kept under a nitrogen atmosphere) were deposited on preheated ITO coverslips and the solvent was evaporated at 20 or 60 °C; both procedures yielded the same results in terms of domain formation and lipid mobility. After adding water into the chamber ($\sim$300 μl), a voltage of 1.1 V at 10 Hz was applied for 1 h. After lipid swelling, the chamber was put either directly at room temperature or cooled down slowly by using a heat block. Both cooling procedures led to the same type of vesicles and domain pattern. Also the presence of the reducing agent dithiothreitol (2 mM, final concentration), to prevent possible lipid oxidation, did not affect domain formation and lipid mobility under our conditions of GUV formation. Whatever procedure was used, the GUVs were always prepared from fresh lipid mixtures and kept under a nitrogen atmosphere as much as possible. Lipids were checked for oxidation by UV/VIS spectroscopy and thin layer chromatography. Under the conditions of GUV preparation, it was found that less than 0.1% of lipids were oxidized.

DiI-C$_{18}$ was added in the amount of 0.1 mol% for confocal imaging and 0.001 mol% for FCS. Since GM1 is known to change the lipid spatial distribution above 2 mol% (44, 45), the compound was used here in minimal amounts, for confocal imaging (0.1 mol%) and FCS (0.05 mol%).

Confocal Fluorescence Microscopy and FCS—Confocal fluorescence microscopy and FCS were performed on a commercial ConfoCor2 (Zeiss, Jena, Germany). Confocal images were taken with the laser scanning microscopy (LSM) module. The excitation light of an Ar ion laser at 488 nm and of a HeNe laser at 543 nm was reflected by a dichroic mirror (HFT 488/543) and focused through a Zeiss C-Apochromat 40×, NA = 1.2 water immersion objective onto the sample. The fluorescence emission was recollected by the same objective and split by another dichroic mirror (NFT 545) into two channels. Detection of the fluorescence emission, after passing a 505–530-nm bandpass filter in the first channel and a 560-nm longpass filter in the second channel, was obtained with two photomultipliers (PMTs). The confocal geometry was ensured by pinholes (60 μm) in front of the PMTs. FCS measurements were performed by epi-illuminating the sample with the 543 nm HeNe laser ($I_{\text{ex}} \approx$ 1.2 kW/cm^2). The excitation light was reflected by a dichroic mirror (HTF 543) and focused onto the sample by the same objective as for the LSM. The fluorescence emission was recollected back and sent to an avalanche photodiode via a 560–615-nm bandpass filter. Out-of-plane fluorescence was reduced by a pinhole (90 μm) in front of the detector. The laser focus was positioned on the topside/bottomside of GUVs, by performing an axial (z-) scan through the membrane prior to the FCS recording. The fluorescence temporal signal was recorded and

the autocorrelation function $G(\tau)$ was calculated, according to Magde *et al.* (44). The apparatus was calibrated by measuring the known three-dimensional diffusion coefficient of rhodamine in solution. The detection area on the focal plane was approximated to a Gaussian profile and had a radius of $\approx$0.18 μm at 1/e^2 relative intensity. Data fitting was performed with the Levenberg-Marquardt nonlinear least-squares fit algorithm (ORIGIN, OriginLab, Northampton, MA). The fitting equation made use of a two-dimensional Brownian diffusion model, assuming a Gaussian beam profile as shown in Equation 1,

$$G(\tau) = \frac{\left[\sum_i \langle C_i \rangle \left[\frac{1}{1 + \tau/\tau_{d,i}} \right] \right]}{A_{eff} \left[\sum_i \langle C_i \rangle \right]^2}, \qquad \text{(Eq. 1)}$$

where $\langle C_i \rangle$ is the two-dimensional time average concentration of the species i in the detection area A_{eff} and $\tau_{d,i}$ is the average residence time of the species i. The diffusion coefficient D_i for the species i is proportional to $\tau_{d,i}$. For FCS measurements, three independent GUVs preparations were analyzed and, for each of them, data from at least 20 different GUVs were recorded with 100 s acquisition time per FCS measurement. When membrane phase separation was visualized with the LSM, the laser focus was always positioned onto one phase only for the FCS experiment.

RESULTS

Lipid Domain Visualization by Confocal Fluorescence Microscopy—Confocal fluorescence microscopy was employed to visualize phase separation in GUVs prepared from SM/DOPC/cholesterol and imaged at room temperature. We exploited the ability of a fluorescent marker, DiI-C$_{18}$, to partition differently in such type of domains. DiI-C$_{18}$ has been used in mixtures of saturated phospholipids and shown to partition preferentially with saturated, long-tailed phospholipids, *e.g.* dipalmitoyl-phosphatidylcholine-phases over coexisting fluid phases by a factor of $\sim$3 (45). We show here that DiI-C$_{18}$ is excluded from the sphingolipid-rich phase and rather favors the DOPC-rich phase. The unambigous phase assignment was carried out by determining the partitioning of GM1, a ganglioside frequently used to identify sphingolipid-enriched rafts (46). Upon incubation of GUVs with the AlexaFluor conjugate of cholera toxin B subunit (AF-CTB), for which GM1 is the natural receptor, the complex GM1-CTB was detected only in areas from which DiI-C$_{18}$ was strongly excluded (SM-enriched). Fig. 1 shows a series of confocal images of GUVs with different lipid compositions and well illustrates the lipid organization and domain morphology when the fraction of cholesterol is varied. GUVs made of pure DOPC exhibited uniform DiI-C$_{18}$ fluorescence (Fig. 1*A*). Here, the lipids were in the fluid phase at room temperature, as following photobleaching of a spot, a quick recovery of fluorescence was observed. GUVs prepared from pure SM were, within the optical resolution, also uniformly fluorescent, but in this case the membrane was in the solid state, at room temperature. Consistently, following photobleaching, no significant recovery of fluorescence was observed within hours (see Fig. 1*B*). Uniform fluorescence was also observed in bilayers formed from DOPC/SM (0.5/0.5 molar ratio) (not shown). However, inclusion of as little as 10 mol% of cholesterol in the SM/DOPC (0.5/0.5) bilayer, sufficed to induce lipid segregation, as evidenced by the preferential partitioning of DiI-C$_{18}$ in one phase (*red areas* in Fig. 1*C*). Strikingly, the marker partitioned in the fluid-disordered phase by a factor of $\sim$50, assuming the quantum efficiency of DiI-C$_{18}$ was the same in both lipid phases. Alexa-Fluor-labeled cholera toxin AF-CTB bound to areas in the GUVs, from which DiI-C$_{18}$ was excluded and formed fluorescent regions exactly complementary to the ones covered by DiI-C$_{18}$ (*green areas* in Fig. 1*C*). The size of SM-enriched domains could vary from a few microns up to a size covering almost half of a 20 μm-sized GUV. Unilamellarity
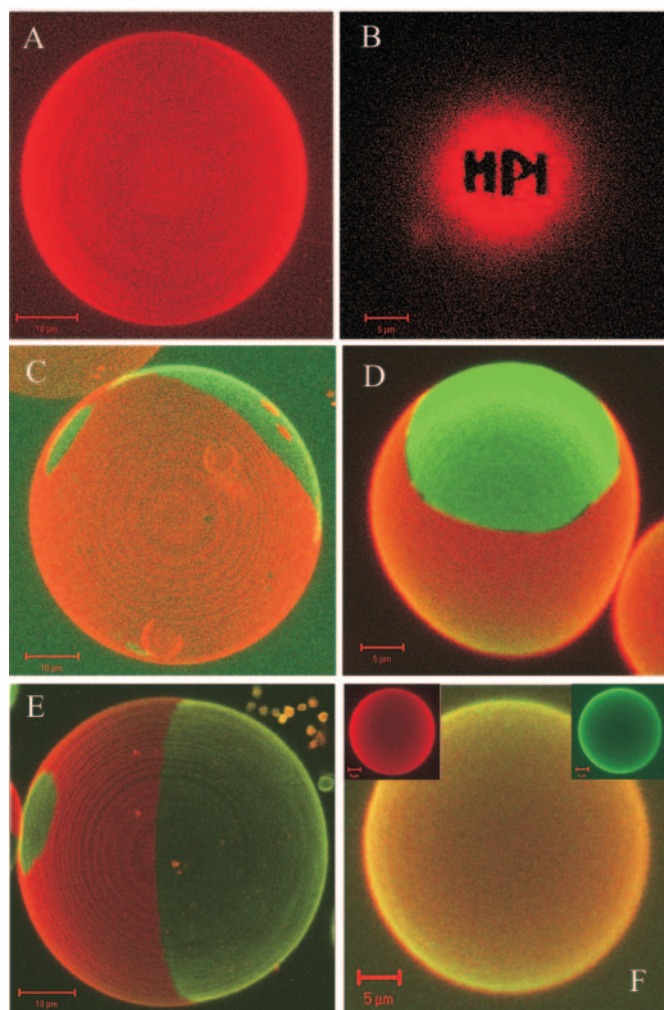
FIG. 1. **Confocal images of giant unilamellar vesicles.** *A*, confocal image at the equator of a GUV (DOPC with 0.1 mol% DiI-C$_{18}$) showing a homogeneous fluorescence corresponding to a single fluid phase. *B*, topside of a GUV (SM with 0.1 mol% DiI-C$_{18}$): after photobleaching of a spot, the fluorescence did not recover within hours, revealing the presence of a single gel-phase. *C–E*, visualization of phase separation for ternary lipid mixtures of SM/DOPC/cholesterol. The dual-color images represent three-dimensional projections of GUVs reconstructed from confocal slices (~0.4-μm thick) with the Zeiss software of ConfoCor2. Increasing cholesterol concentrations with SM/DOPC 0.5/0.5 are shown: *C*, 10 mol%; *D*, 20 mol%; *E*, 33 mol%. DiI-C$_{18}$ (*red channel*) strongly favored the DOPC-enriched, fluid-disordered phase, whereas AF-CTB (*green channel*) bound to GM1 in GUV areas, from which DiI-C$_{18}$ was excluded. Note that the total green surface increased with increasing cholesterol concentration. The domains were always round and their sizes varied between 1 and 10 μm. *F*, a further increase in cholesterol concentration (50 mol%) yielded confocal images identical in appearance to *A*. Here, fluorescence from DiI-C$_{18}$ (see *inset*, *red*) and GM1-bound AF-CTB bound (see *inset*, *green*) was homogeneously distributed, indicating either a single phase or heterogeneity at dimensions beyond the optical resolution (~0.3 μm).

of the vesicles allowed us to look for phase interlayer coupling and it was found that, in all of the GUVs, the phase domains comprised both apposing membrane leaflets. Phase separation was also visualized at higher amounts of cholesterol (SM/DOPC = 0.5/0.5), as shown in Fig. 1*D* for 20 mol% and in Fig. 1*E* for 33 mol% of cholesterol. The domain morphology was the same as described for 10 mol% cholesterol, except that the total surface area of the SM-enriched phase increased with the amount of cholesterol. At 50 mol% cholesterol, rafts were no longer observed within the optical resolution (Fig. 1*F*). Similarly, uniform fluorescence from DiI-C$_{18}$ and GM1-bound AF-

CTB was detected in GUVs with 65 mol% cholesterol (not shown).

Membrane Lipid Mobility Is Controlled by Cholesterol—We assessed the membrane lipid mobility of GUVs made from ternary mixtures of DOPC/SM/cholesterol by measuring the diffusion coefficient of DiI-C$_{18}$ by FCS. In Fig. 2*A*, correlation curves are shown for the liquid-disordered, DOPC-enriched domain, where DiI-C$_{18}$ preferentially partitioned, and in Fig. 2*B* those for the liquid-ordered, SM-enriched domain, from which DiI-C$_{18}$ was largely excluded. Note that the sensitivity of FCS allows one to measure lipid diffusion with the fluorescent marker at very low concentrations in both phases. As soon as phase separation occurred, in the presence of 10 mol% of cholesterol (Fig. 2*A*, *dash* (*d*)), the lipid mobility in liquid-disordered domains ($D = 4.9 \pm 0.3 \times 10^{-8}$ cm^2/s) almost matched the one of pure DOPC membranes ($D = 6.3 \pm 0.2 \times 10^{-8}$ cm^2/s, Fig. 2*A*, *dot* (*a*)). This mobility was significantly higher than that measured in DOPC/SM (0.5/0.5) GUVs in the absence of cholesterol ($D = 2.6 \pm 0.2 \times 10^{-8}$ cm^2/s, Fig. 2*A*, *solid* (*e*)). An increase in the cholesterol concentration hardly affected the mobility value of DiI-C$_{18}$ relative to values measured for pure DOPC. On the other hand, cholesterol greatly varied the lipid mobility in the SM-enriched phase (Fig. 2*B*), where lipid diffusion was significantly slower than in the fluid-disordered phase and in the SM/DOPC (0.5/0.5) mixture without cholesterol (Fig. 2*B*, *solid* (*a*)). However, by increasing the amount of cholesterol, the membrane lipid mobility in SM-enriched domains greatly increased, from $D = 0.105 \pm 0.031 \times 10^{-8}$ cm^2/s (10 mol% cholesterol, Fig. 2*B*, *dash* (*f*)) up to $D = 0.795 \pm 0.108 \times 10^{-8}$ cm^2/s (33 mol% cholesterol, Fig. 2*B*, *dash dot dot* (*d*)) approaching that of SM/DOPC (0.5/0.5) mixtures. By further increasing the amount of cholesterol, the domains disappeared but the lipid mobility remained higher than that of the SM-rich domains (50 mol% cholesterol, Fig. 2*B*, *short dash* (*b*)), though lower than in SM/DOPC = 0.5/0.5 GUVs. Any further increase in cholesterol concentration made the whole membrane stiffer (*e.g.* 65 mol% cholesterol in Fig. 2*B*, *short dash dot* (*c*)). Taking different SM/PC molar ratios ≥ 1 (*e.g.* 0.53/0.13), the domain morphology and the lipid diffusion were unchanged (see Table I). On the other hand, in the case of SM/PC molar ratios < 1, no domains were visualized by confocal microscopy and the lipid dynamics measured was rather high and very close to that in pure DOPC (*e.g.* SM/DOPC 0.13/0.53, see Table I). For all of the FCS curves, excellent fits were produced with a one-component normal Brownian diffusion model (37). The diffusion coefficients, calculated from the fitting of FCS curves shown in Fig. 2, are reported as a function of mol% of cholesterol in Fig. 3 (see also Table I).

Lipid Mobility in Binary Mixtures—In order to investigate in more detail the lipid spatial organization in raft-exhibiting membranes, lipid mobility in GUVs prepared from ternary mixtures of SM/DOPC/cholesterol was compared with that in GUVs from binary mixtures of DOPC/cholesterol, SM/cholesterol and DOPC/SM. For all of these binary compositions, GUVs showed no phase separation by confocal microscopy. The FCS measurements of DiI-C$_{18}$ mobility could be well fitted with a one diffusion-component. In Fig. 4*A*, FCS curves recorded for DOPC/cholesterol membranes are shown. The diffusion coefficients obtained from the fitting are plotted as a function of cholesterol concentration in Fig. 4*B*: a gradual shift of lipid mobility toward lower values is observed upon increase of the amount of cholesterol. Compared with DOPC/cholesterol mixtures, the opposite effect of the cholesterol was observed in SM/cholesterol mixtures, where the lipid mobility increased upon increase of mol% of cholesterol (see FCS curves in Fig. 4*C* and the corresponding diffusion coefficients reported as a func-
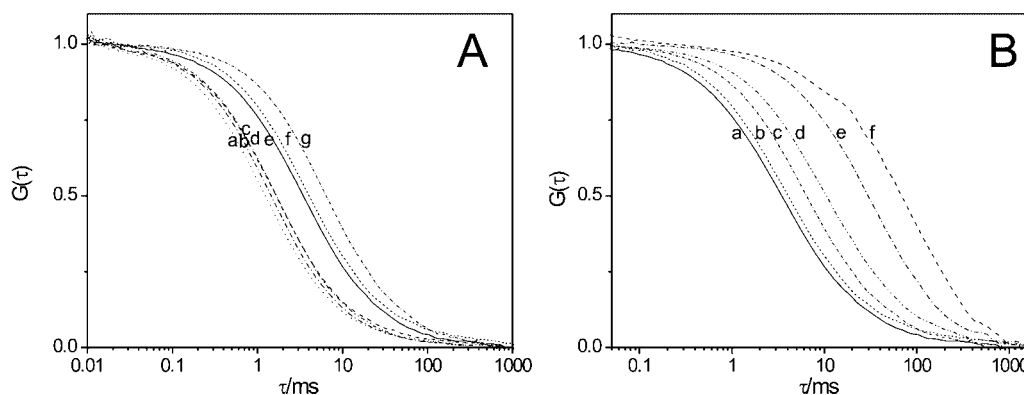
FIG. 2. **Ternary lipid mixtures of SM/DOPC/cholesterol exhibit phase separation.** *A*, FCS curves were recorded for the fluid-disordered, DOPC-enriched phase at increasing cholesterol concentration (*dash* (*d*) indicates 10 mol%, *dash dot* (*c*) indicates 20 mol%, and *dash dot dot* (*b*) indicates 33 mol%). The correlation decays almost matched the one from GUVs of pure DOPC (*dot*, *a*) and were much faster than those from GUVs of SM/DOPC = 0.5/0.5 (*solid*, *e*), of SM/DOPC = 0.5/0.5 with 50 mol% (*short dash*, *f*) or 65 mol% of cholesterol (*short dash dot*, *g*). *B*, FCS curves were recorded for the fluid-ordered, SM-enriched phase at increasing cholesterol concentration (*dash* (*f*) indicates 10 mol%, *dash dot* (*e*) indicates 20 mol%, and *dash dot dot* (*d*) indicates 33 mol%). *Short dash* (*b*) indicates 50 mol% cholesterol, *short dash dot* (*c*) 65 mol% cholesterol, and solid (*a*) SM/DOPC = 0.5/0.5.

TABLE I

Translational diffusion coefficients for the ternary SM/DOPC/cholesterol system

Values of diffusion coefficient of DiI-C$_{18}$, as obtained from the fitting of FCS curves, in GUVs prepared from DOPC/SM/cholesterol mixtures (see "Materials and Methods").

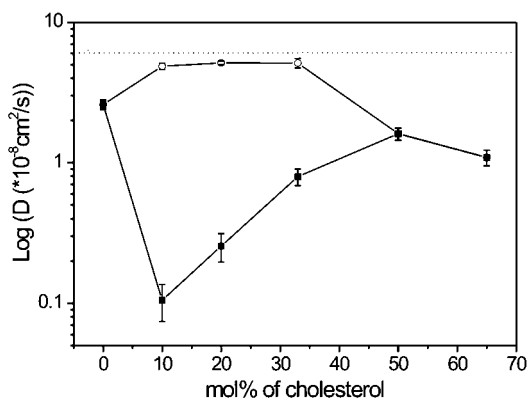| Composition, molar fraction			No phase separation	Phase separation	
SM	DOPC	Chol	D	D_{ld}	D_{lo},
			$\times 10^{-8}\ cm^2/s$	$\times 10^{-8}\ cm^2/s$	$\times 10^{-8}\ cm^2/s$
1	0	0	immoble	-	
0	1	0	6.3 ± 0.2	-	
0.5	0.5	0	2.6 ± 0.2	-	
0.45	0.45	0.1		4.9 ± 0.3	0.105 ± 0.031
0.4	0.4	0.2		5.15 ± 0.15	0.255 ± 0.058
0.33	0.33	0.33		5.1 ± 0.4	0.795 ± 0.108
0.25	0.25	0.5	1.6 ± 0.2		
0.175	0.175	0.65	1.1 ± 0.1		
0.1	0.8	0.1	4.9 ± 0.4		
0.13	0.53	0.33	4.6 ± 0.4		
0.53	0.13	0.33		5.1 ± 0.9	0.8 ± 0.1

FIG. 3. **Average diffusion coefficients, as determined from fitting the autocorrelation curves in Fig. 2, *A* and *B*, as a function of cholesterol concentration.** Values for the DOPC-enriched phase are indicated by *open circles*, those for the SM-enriched phase and for mixtures that do not give rise to phase separation (within the optical resolution) are indicated by *filled squares*. The *dashed line*, which corresponds to the value of lipid diffusion coefficient in GUVs of DOPC, is shown as a reference.

tion of mol% of cholesterol in Fig. 4*D*). For binary mixtures of SM/DOPC, phase separation was observed by confocal microscopy for mol% of SM ≥ 80%. DiI-C$_{18}$ favored the SM/DOPC gel-phase, with a partition coefficient of ∼ 3. In Fig. 4*E* the FCS curves and in Fig. 4*F* the corresponding diffusion coefficients of

DiI-C$_{18}$ are reported for GUVs composed of SM/DOPC at different ratios. For the data at 80 mol% SM, only FCS curves in the less bright fluid-disordered regions could be recorded, as the FCS measurements in the SM gel-phase were strongly affected by photobleaching. These latter results confirm that, in SM/DOPC membranes with ≥ 80 mol% of SM, an equilibrium is established at room temperature between a SM-enriched gel-phase and a SM/DOPC-containing, liquid-disordered phase characterized by high lipid mobility.

Phase Diagram—The FCS measurements were used to build the phase diagram shown in Fig. 5. Starting from the left axis (DOPC/cholesterol), the membrane lipid mobility continuously decreases upon increase of cholesterol concentration. Consistent with previous findings for phospholipid/cholesterol mixtures (23, 47), a transition from liquid-disordered to liquid-ordered phase can be identified around ∼40 mol% of cholesterol. As the lipid diffusion coefficients in DOPC-enriched domains of DOPC/SM/cholesterol GUVs almost match that of pure DOPC, we can conclude that the DOPC-enriched phase is largely devoid of cholesterol and that the SM-enriched phase takes up most, if not all, of the cholesterol present in the membrane. The slight mismatch could be simply due to the presence of small amounts (∼5–10%) of SM/cholesterol clusters in the DOPC-rich phase. In contrast to DOPC membranes, lipid dynamics in SM membranes (*right axis* in Fig. 5) increases upon addition of cholesterol and undergoes a transition from gel-phase to a liquid-ordered phase around 40 mol% of choles-
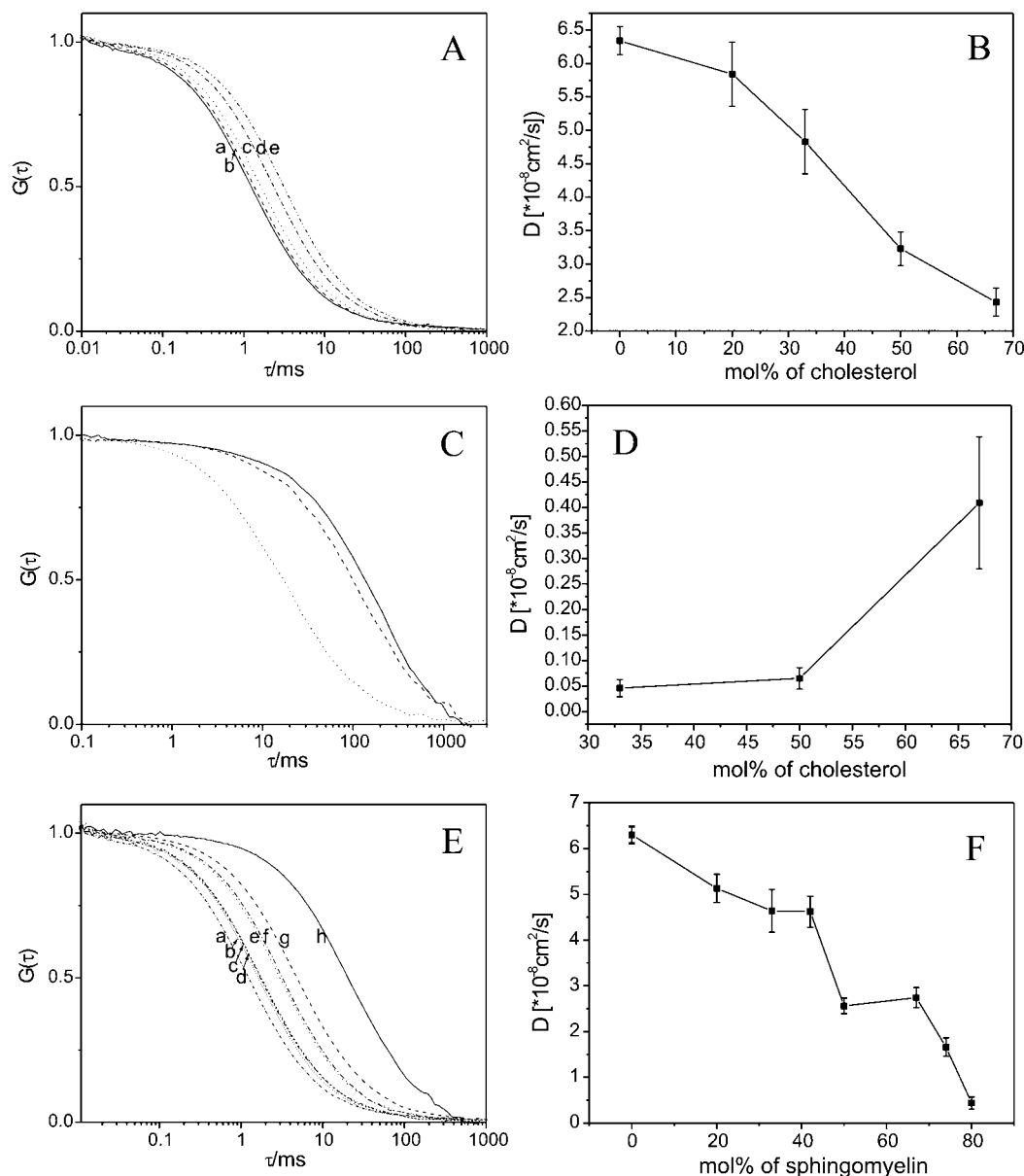
FIG. 4. **Binary mixtures of DOPC/cholesterol and SM/cholesterol exhibit a continuous change in diffusion coefficient as a function of cholesterol concentration.** Lipid mobility in GUVs prepared from the DOPC/SM mixture decreased as a function of SM concentration. *A*, FCS autocorrelation curves are shown for DiI-C$_{18}$ mobility in DOPC/cholesterol GUVs, *solid line* (*a*) for 0 mol%, *dash* (*b*), for 20 mol%, *dot* (*c*) for 33 mol%, *dash dot* (*d*) for 50 mol%, and *dash dot dot* (*e*) for 67 mol% of cholesterol. *B*, average diffusion coefficients, as determined from the fitting of the autocorrelation curves in *A*, are reported as a function of cholesterol concentration. *Bars* represent the S.D. from the average values (see "Materials and Methods" for details). *C*, FCS autocorrelation curves are shown for DiI-C$_{18}$ mobility in SM/cholesterol GUVs, in *solid* for 33 mol%, *dash* for 50 mol%, *dot* for 67 mol% cholesterol. In the absence of cholesterol, SM was in the gel-phase and the lipid translational mobility is virtually zero (see Fig. 1*B*). The lipid mobility at ≤20 mol% cholesterol was too low to be measured by FCS. *D*, average diffusion coefficients, as determined from the fitting of the autocorrelation curves in *C*, are reported as a function of cholesterol concentration. *Bars* represent the S.D. from the average values (see "Materials and Methods" for details). *E*, FCS autocorrelation curves are shown for DiI-C$_{18}$ mobility in DOPC/SM GUVs, *short dash dot* (*a*) for 0 mol%, *short dot* (*b*) for 20 mol%, *short dash* (*c*) for 33 mol%, *dash dot dot* (*d*) for 42 mol%, *dash dot* (*f*) for 50 mol%, *dot* (*e*) for 67 mol%, *dash* (*g*) for 74 mol%, and *solid* (*h*) for 80 mol% SM. *F*, average diffusion coefficients, as determined from fitting of the autocorrelation curves in *E*, are reported as a function of SM concentration. *Bars* represent the S.D. from the average values (see "Materials and Methods" for details).

terol. The trend of diffusion coefficients is comparable to that of the SM-rich phase in DOPC/SM/cholesterol GUVs and, remarkably, much steeper than what estimated in previous reports (31, 32). However, the values of diffusion coefficient are larger in the SM-rich areas of ternary mixtures than in the binary SM/cholesterol. Therefore, we can conclude that the liquid-ordered phase in SM/DOPC/cholesterol membranes is mainly composed of SM/cholesterol but, most likely, also contains some DOPC, which further increases the lipid mobility. Finally, the lipid dynamics in DOPC/SM GUVs is regulated by the amount of SM soluble in the fluid DOPC membrane. The

trend of lipid diffusion coefficients as a function of mol% of SM suggests the presence of two transition points, the first being around 10 mol% SM and the second around 45 mol%. The difference in lipid mobility between these ranges may be due to different molecular packing and spatial distributions of gel-phase and liquid-disordered lipid clusters.

DISCUSSION

We have characterized the morphology of raft-like microdomains in GUVs, prepared from ternary mixtures of dioleoyl-phosphatidylcholine (DOPC), sphingomyelin (SM), and choles-
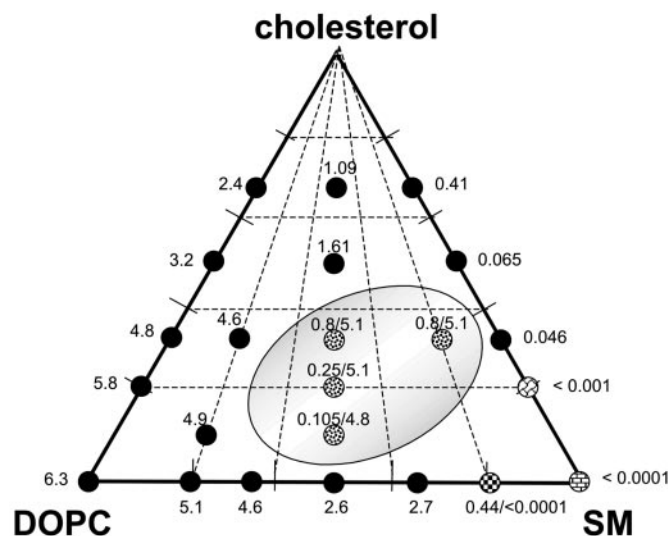
Lipid Dynamics in Domain-forming Membranes

FIG. 5. **Ternary phase diagram for the SM/DOPC/cholesterol system at 25 °C, constructed on the basis of confocal imaging and FCS data.** The enlighted region indicates the areas at which phase separation occurs. By using the lipid diffusion coefficient as a finger-print for the lipid composition, the diagram shows transitions points/lines between different phases, and, more importantly, gives information about changes in membrane lipid mobility, even within a phase region. *Circles* refer to the compositions analyzed in this study (*filled circles* indicate no phase separation visible in the confocal microscope; *dotted circles* indicates coexistence of liquid-disordered and liquid-ordered phases, hence, raft-like domains; *circles with bricks* indicate pure gel-phase; *circles with squares* indicate coexistence of gel-phase and liquid-disordered phase; and *circles with curved lines* indicate coexistence of gel-phase and liquid-ordered phase). *Numbers* next to the *circles* give the average lipid diffusion coefficients ($\times 10^{-8}$ cm^2/s) measured by FCS for a particular composition (see Table I).

terol, by confocal fluorescence microscopy and the lipid dynamics by FCS. Cholesterol promotes phase separation of DOPC-enriched and SM-enriched domains by engaging a stable and strong interaction with SM, as demonstrated by the partitioning of the lipophilic probe DiI-C$_{18}$. Most importantly, cholesterol plays a pivotal role in tuning the lipid mobility, in particular in the SM-enriched domains.

Previously, domains with raft-like properties were visualized by one- and two-photon fluorescence microscopy in model membranes (31, 32). Depletion and repletion of cholesterol in membranes composed of SM/DOPC/cholesterol (1/1/1) resulted in disappearance and reappearance of lipid rafts in supported monolayers (32). However, a systematic investigation of the morphology of raft-like domains as a function of cholesterol concentration has never been attempted. From the confocal images shown here, it is evident that cholesterol is the determining factor in causing phase separation of sphingolipids and unsaturated phospholipids. Confocal images of GUVs made of SM/DOPC (0.5/0.5) and different amounts of cholesterol show that, at room temperature, extended phase separation starts to occur at 10 mol% cholesterol. Consistent with previous studies reporting phase separation in model membranes with similar lipid mixtures (31, 32), the round shape of the domains suggests the coexistence of a liquid-ordered and a liquid-disordered phase, as the circular borders of the domains minimize the line energy. GUVs with less than 10% or more than 50% cholesterol did not exhibit phase separation, at least within the optical resolution. As previously observed in artificial membranes (31, 38), ordered phase domains in apposing leaflets were always perfectly coincident. Therefore, at least in the case of SM/DOPC/cholesterol mixtures, where the long fatty acid chains of SM in opposite leaflets can superimpose by interdigitation, the lipid component alone is able to create strong cou-

pling between inner and outer leaflet.

It has been proposed that cholesterol-rich membranes exhibit formation of a sphingolipid-rich, liquid-ordered phase, which separates from a phospholipid-rich, liquid-disordered phase (1–4). Lipid segregation is driven by the tendency of sphingolipids to engage special molecular interactions with cholesterol and to organize in a more ordered manner than unsaturated phospholipids. By adding a certain amount of cholesterol to the SM/DOPC mixture, the lipophilic probe DiI-C$_{18}$ is squeezed out of the SM-enriched regions and greatly favors the unsaturated phospholipid-enriched domain. In contrast, in GUVs prepared from SM/DOPC mixtures, with ≥ 80 mol% of SM, DiI-C$_{18}$ presents a slight preference for the SM-rich gel-phase.

We have used FCS to systematically analyze lipid mobility and identify the effect of cholesterol in rafts. FCS has been successfully applied to study diffusion of lipids and proteins in membranes (39, 48). Quantitative information on the average number of the particles in focus and their dynamic properties, *e.g.* diffusion coefficients, can be obtained with excellent statistical accuracy (38). FCS has been shown to be sensitive to deviations from single-phase behavior, *e.g.* caused by heterogeneities in the sample (39). As lipid rafts are thought to be dynamic assemblies in membranes, the assessment of lipid dynamic properties is an important step toward the understanding of how lipids modulate membrane lipid mobility and, thereby, possibly control the timing of cellular events, such as sorting or signaling. This technique is less time-consuming than SPT and, in contrast to FRAP, FCS works at single molecule regimes. This is a great advantage in experiments on domain formation in membranes, because of the following. (i) Lipid analogs do not need to be introduced at high amounts, which have been shown to affect, in some cases, the lipid organization (48, 49), and (ii) at a single molecule level, clustering of the dye may be readily spotted. FCS illustrates, here, the important role of cholesterol in tuning the membrane lipid mobility in raft-containing membranes. Consistent with previous studies (32), lipid diffusion in liquid-disordered phase is ~ 2 times faster than in cholesterol devoid GUVs (SM/DOPC 0.5/0.5). However, the most remarkable effect is found for the lipid diffusion in SM-enriched phases, where the mobility increases by a factor of ~ 8 as the cholesterol concentration is increased from 10% up to 33%. This implies that cholesterol acts as raft-promoting component and, most importantly, is able to control the lipid dynamics in domains. On the other hand, the SM level (for SM/DOPC molar ratios ≥ 1) does not affect very much the lipid dynamics in domains. This result might have some physiological implications, as it implies that cells can alter the SM levels without altering the dynamic properties of the domains.

The lipid diffusion coefficient characterizes a certain lipid phase composition, given the data reproducibility, the good statistical accuracy of the results and the excellent properties of GUVs as model membranes. Vesicle unilamellarity ensures that the diffusion components in the autocorrelation curve belong only to molecules diffusing within a single bilayer. On the basis of our data, we constructed a phase diagram for the DOPC/SM/cholesterol mixture. The classic method for studying equilibrium between phases in membranes is Differential Scanning Calorimetry (DSC), often combined with infrared and fluorescence spectroscopy (47). Additional information can be extracted by Atomic Force Microscopy (in the sub-micrometer scale) (46), or one- and two-photon fluorescence microscopy (in the μm scale) (30–32). These techniques describe the static lipid organization, whereas, here, we exploit the time dimension and use the dynamic parameters obtained by FCS as a

fingerprint for membrane phases. We have identified regions of lipid compositions that give rise to phase separation and obtained information on the phase transition points. A large amount of literature has been previously reported on phase diagrams of similar ternary systems (Refs. 47 and 51, see Ref. 52 for an excellent review). Our data on lipid dynamics add new information as we show how membrane lipid mobility changes, not only between different phase regions but also within a particular region.

In conclusion, FCS has been proven to be a valuable tool to assess the molecular basis of lipid mobility in raft-like domains, which is crucial for our understanding of the dynamics of many biological processes. Here, we focused on the role of cholesterol in promoting phase separation and increasing the lipid mobility in SM-enriched phases. In addition, by using the dynamic parameters obtained by FCS, we built a phase diagram, which reports on the lipid dynamic properties within different lipid phases.

REFERENCES

1. Simons, K., and van Meer, G. (1988) *Biochemistry* **27,** 6197–6202
2. Sankaram, M. B., and Thompson, T. E. (1990) *Biochemistry* **29,** 10670–10675
3. Simons, K., and Ikonen, E. (1997) *Nature* **387,** 569–572
4. Brown, D. A., and London, E. (1998) *Annu. Rev. Cell Dev. Biol.* **14,** 111–136
5. Robinson, P. J. (1991) *Immunol. Today* **12,** 35–41
6. Stulnig, T. M., Berger, M., Sigmund, T., Stockinger, H., and Horejsi, V. (1997) *J. Biol. Chem.* **272,** 19242–19247
7. Germain, R. N. (1997) *Curr. Biol.* **7,** R640–644
8. Field, K. A., Holowka, D., and Baird, B. (1995) *Proc. Natl. Acad. Sci. U. S. A.* **92,** 9201–9205
9. Field, K. A., Holowka, D., and Baird, B. (1997) *J. Biol. Chem.* **272,** 4276–4280
10. Sheets, E. D., Holowka, D., and Baird, B. (1999) *J. Cell Biol.* **145,** 877–887
11. Brown, D. A., and Rose, J. K. (1992) *Cell* **68,** 533–544
12. Ikonen, E. (2001) *Curr. Opin. Cell Biol.* **13,** 470–477
13. Dotti, C. G., Parton, R. G., and Simons, K. (1991) *Nature* **349,** 158–161
14. Anderson, R. G. (1998) *Annu. Rev. Biochem.* **67,** 199–225
15. Smart, E. J., and Anderson, R. G. (1999) *Mol. Cell. Biol.* **19,** 7289–7304
16. Bretscher, M. S., and Munro, S. (1993) *Science* **261,** 1280–1281
17. Sevinsky, J. R., Rao, L. V. M., and Ruf, W. (1996) *J. Cell Biol.* **133,** 293–304
18. Stang, E., Kartenbeck, J., and Parton, R. G. (1997) *Mol. Biol. Cell.* **8,** 47–57
19. Brown, D. A., and London E. (2000) *J. Biol. Chem.* **275,** 17221–17224
20. Schmidt, C. F., Barenholz, Y., Huang, C., and Thompson, T. E. (1978) *Nature* **271,** 775–777
21. Fridriksson, E. K. (1999) *Biochemistry* **38,** 8056–8063
22. Brown, R. E. (1998) *J. Cell Sci.* **111,** 1–9
23. Brown, D. A., and London, E. (1998) *J. Membr. Biol.* **164,** 103–114
24. Brown, D. A. (2001) *Proc. Natl. Acad. Sci. U. S. A.* **98,** 10517–10518
25. Heerklotz, H. (2002) *Biophys. J.* **83,** 2693–2701
26. Wilson, B. S., Pfeiffer, J. R., and Oliver, J. M. (2000) *J. Cell Biol.* **149,** 1131–1142
27. Varma, R., and Mayor, S. (1998) *Nature* **394,** 798–801
28. Kenworthy, A. K., Petranova, N., and Edidin, M. (2000) *Mol. Biol. Cell* **11,** 1645–1655
29. Schütz, G. J., Kada, G., Pastushenko, V. P., and Schindler H. (2000) *EMBO J.* **19,** 892–901
30. Bagatolli, L. A., and Gratton, E. (2000) *Biophys. J.* **78,** 290–305
31. Dietrich, C., Bagatolli, L. A., Volovyk, Z. N., Thompson, N. L., Levi, M., Jacobson, K., and Gratton, E. (2001) *Biophys. J.* **80,** 1417–1428
32. Dietrich, C., Volovyk, Z. N., Levi, M., Thompson, N. L., and Jacobson K. (2001) *Proc. Natl. Acad. Sci. U. S. A.* **98,** 10642–10647
33. Samsonov, A. V., Mihalyov, I., and Cohen, F. C. (2001) *Biophys. J.* **81,** 1486–1500
34. Simons, K., and Toomre, D. (2000) *Nat. Rev. Mol. Cell. Biol.* **1,** 31–39
35. Fujiwara, T., Ritchie, K., Murakoshi, H., Jacobson, K., and Kusumi, A. (2002) *J. Cell Biol.* **157,** 1071–1081
36. Eigen, M., and Rigler, R. (1994) *Proc. Natl. Acad. Sci. U. S. A.* **91,** 5740–5747
37. Schwille, P. (2001) *Cell Biochem. Biophys.* **34,** 383–408
38. Koppel, D. E. (1974) *Phys. Rev. A* **10,** 1938–1945
39. Korlach, J., Schwille, P., Webb, W. W., and Feigenson, G. (1999) *Proc. Natl. Acad. Sci. U. S. A.* **96,** 8461–8466
40. Angelova, M. I., and Dimitrov, D. S. (1986) *Faraday Discuss. Chem. Soc.* **81,** 303–308
41. Dimitrov, D. S., and Angelova, M. I. (1988) *Bioelectrochem. Bioenerg.* **19,** 323–333
42. Menger, F. M., and Angelova, M. I. (1998) *Acc. Chem. Res.* **31,** 789–797
43. Mathivet, L., Cribier, S., and Devaux, P. F. (1996) *Biophys. J.* **70,** 1112–1121
44. Magde, D., Elson, E., and Webb, W. W. (1972) *Phys. Rev. Lett.* **29,** 705–708
45. Spink, C. H., Yeager, M. D., and Feigenson, G. W. (1990) *Biochim. Biophys. Acta* **1023,** 25–33
46. Harder, T., Scheiffele, P., Verkade, P., and Simons, K. (1998) *J. Cell Biol.* **141,** 929–942
47. Silvius, J. R., del Giudice, D., and Lafleur, M. (1996) *Biochemistry* **35,** 15198–15208
48. Schwille, P., Korlach, J., and Webb, W. W. (1999) *Cytometry* **36,** 176–182
49. Yuan, C., Furlong, J., Burgos, P., and Johnston, L. J. (2002) *Biophys. J.* **82,** 2526–2535
50. Yuan, C., and Johnston, L. J. (2000) *Biophys. J.* **79,** 2768–2782
51. Feigenson, G. W., and Buboltz, J. T (2001) *Biophys. J.* **80,** 2775–2788
52. McConnell, H. M., and Vrljic, M. (2003) *Annu. Rev. Biophys. Biomol. Struct.* **32,** 469–492